Using quantitative intravital multiphoton microscopy to dissect hepatic transport in rats

Kenneth W. Dunn and Jennifer C. Ryan

Department of Medicine
Division of Nephrology
Indiana University School of Medicine
Indianapolis, IN 46202

Address Correspondence to:

Ken Dunn
Phone: 317-278-0436
Email: kwdunn@iu.edu

This is the author's manuscript of the article published in final edited form as:

Dunn, K. W., & Ryan, J. C. (2017). Using quantitative intravital multiphoton microscopy to dissect hepatic transport in rats. Methods. https://doi.org/10.1016/j.ymeth.2017.04.015

Abstract

Hepatic solute transport is a complex process whose disruption is associated with liver disease and drug-induced liver injury. Intravital multiphoton fluorescence excitation microscopy provides the spatial and temporal resolution necessary to characterize hepatic transport at the level of individual hepatocytes *in vivo* and thus to identify the mechanisms and cellular consequences of cholestasis. Here we present an overview of the use of fluorescence microscopy for studies of hepatic transport in living animals, and describe how we have combined methods of intravital microscopy and digital image analysis to dissect the effects of drugs and pathological conditions on the function of hepatic transporters *in vivo*.

Key words

Intravital microscopy, digital image analysis, fluorescence microscopy, in vivo imaging, cholestasis, liver injury

1. Introduction

A primary function of the liver is to regulate the constitution of the blood, mediating the metabolism and excretion of endogenous and exogenous compounds. The critical role of these processes is demonstrated by the serious pathologies associated with mutations in the proteins that mediate hepatic metabolism and transport. Hepatic transport is of particular interest in pharmaceutical development. In addition to mediating the metabolism and clearance of drugs, the liver is frequently the victim of off-target drug effects. In particular, drug-induced liver injury, one of the most expensive and vexing problems in drug development, is associated with drugs that inhibit hepatocyte secretory function [1-3].

The transport of drugs and metabolites is accomplished by proteins that mediate transport from the sinusoid capillaries into the hepatocyte cytosol, from the hepatocyte cytosol to the bile canaculi or from the hepatocyte cytosol back into the sinusoids. The major uptake transporters include proteins of the Solute Carrier family, e.g. OATP (SLC01A2, SLC21A6 SLC21A8, SLC21A9), OCT (SLC22A1) and NTCP (SLC10A1). Major secretory transporters include proteins of the ATP-binding Cassette transporter family, such as MRP2 (ABCC2), MDR3 (ABCB4) and BSEP (ABCB11), which mediate canalicular secretion) and MRP3 (ABCC3) and MRP4 (ABCC4), which mediate sinusoidal reflux back into the blood). Drugs may impact one or more of these transporters in such a way as to increase or decrease the metabolism and clearance of drugs and metabolites. Furthermore, depending upon the balance of effects on uptake and secretory transporters, a cholestatic drug may induce the accumulation of a drug or toxic metabolite in the hepatocyte cytosol, inducing liver injury. It is thus critical to not only determine that a drug disrupts normal liver transport, but also to determine the site(s) of transport disruption.

While the effects of drugs on the function of specific transporters can be sensitively measured in studies of isolated membrane vesicles, the additional complexity of the *in vivo* situation makes it difficult to extrapolate these measurements to predictions of in vivo effects, particularly since local *in vivo* drug concentrations are typically unknown. Transport can also be evaluated in studies of cultured cells. While hepatocytes grown in vitro recapitulate many *in vivo* functions, particularly when grown in sandwich culture, results obtained from these systems can also be difficult to extrapolate to the *in vivo* condition. First, depending upon culture conditions, transporter expression levels change to varying degrees after isolation. Second, cultured cells lack the structure of the lobule, a transport unit in itself that is organized such that substrates are sequentially transported and metabolized by hepatocytes with different and independently-regulated populations of transporters [4-8]. Third, these simple systems lack the systemic inputs that dynamically regulate the abundance and distribution of hepatic transporters *in vivo* [9-13], making them incapable of reproducing the complex circumstances of pathological conditions, such as infection.

Conversely, the standard imaging and biochemical approaches used in animal studies can detect cholestasis, but provide only indirect evidence as to underlying mechanisms. The ideal system for dissecting hepatic transport would provide the spatial and temporal resolution necessary to distinguish the individual steps of transport, but in the relevant physiological context, consisting of differentiated hepatocytes in the multi-cellular environment of the intact liver lobule, with intact vascular, immune and endocrine inputs. In addition to

supporting dissection of drug effects under physiological conditions, such a system would support studies of the effects of pathology on liver transport and studies of the effects of drugs in the context of pathology.

Studies of isolated and cultured hepatocytes have demonstrated that fluorescence microscopy provides the spatial and temporal resolution necessary to characterize transport of fluorescent probes [14-17]. The same general approach can be applied to studies of hepatic transport *in vivo* using intravital microscopy of the liver of laboratory animals. As early as 1945, a crude fluorescence microscope system was used to study the effects of various insults on transport of fluorescein in the rat liver [18]. Approximately 40 years later, digital epifluorescence microscopy was used to characterize transport of fluorescein and fluorescein-glycocholate in the livers of rats and hamsters [19, 20]. In the past twenty years, investigators have capitalized on the increased reach and resolution of multiphoton fluorescence excitation microscopy to evaluate transport of fluorescein and other fluorescent probes in rats [21-26] and mice [27, 28]. **Figure 1** shows an example of a multiphoton fluorescence excitation image collected from the liver of a rat 20 minutes after intravenous injection of rhodamine dextran (retained in the vasculature) and sodium fluorescein (transported into hepatocytes and bile canaliculi). The inset demonstrates that the resolution provided by multiphoton microscopy is sufficient to clearly resolve sinusoids, hepatocytes and bile canaliculi. Here we describe how we have combined methods of intravital microscopy and image analysis to quantify the effects of drugs and disease on l transport *in vivo.*

2. Approach

2.1 Overview - The intravital microscopy transport assays described here are based upon quantitative analysis of images collected in time series from the liver of a living rodent following intravenous injection of fluorescent transport substrates, largely following previously described approaches [22, 23]. Images collected in this way demonstrate that fluorescein uptake and secretion proceed very rapidly. **Figure 2** shows that within a minute of perfusion, detectible levels of fluorescein are present not only in the hepatocyte cytosol, but also in bile canaliculi. Within 6 minutes of perfusion, a substantial amount of fluorescein has already been transported into canaliculi. Panel F shows that fluorescein secretion into canaliculi is essentially blocked in rats treated with the cholestatic agent taurolithocholate (TLC). The 10 minute time course of fluorescein transport in the presence or absence of TLC is shown in **Video 1.**

2.2 Surgical preparation and presentation of the rat liver on the microscope stage - All studies described here were approved and conducted according to the Institutional Animal Care and Use Committee guidelines of Indiana University, and adhere to the guide for the care and use of animals [29]

Experimental animals are typically acclimatized for a period of at least 4 days and, depending upon the study, fasted for 16 hrs prior to studies. Adult Sprague Dawley (or Wistar) rats, weighing between 180 and 400 grams, are sedated with 5% Isoflurane, weighed and 130mg/kg Inactin is administered intraperitoneally for anesthesia. Anesthesia is monitored by evaluation of responses to gentle pinching of ears and feet. The rat is placed on a heating pad to maintain body temperature. Body temperature is monitored using a rectal thermometer, and heart rate and respiratory rate are monitored visually.

Once anesthetized, a 3 x 1.5 cm, L-shaped incision is made 1 cm to the right of the ventral midline in the neck. A jugular cannula is then placed using PE 50 tubing filled with sterile 0.9% saline and attached to a Luer stub adapter and 1 mL syringe. The neck is sutured with 3-0 black silk sterile suture. At this time, a bolus of Hoechst 33342 (Invitrogen, 2 mg/kg) diluted in 0.9% sterile saline to a total volume of 0.4 mL is injected into the jugular line to label cell nuclei [30].

The liver is exposed for imaging by making a 4 cm incision across the torso 1 to 2 cm below the middle of the rib cage. A wet (0.9% saline) 2x2 gauze sponge is gently placed below the left lateral liver lobe. In order to minimize tissue motion for microscopy, the liver is tethered to the bottom of a 50 mm Willco coverslip-bottomed dish (GWST-5040, Warner Instruments, Hamden, Ct). Tape is placed on the periphery of the glass window of the dish, and cyanoacrylate glue is applied to the tape. The glass window is pressed to the liver and the gauze on either side of the liver is gently pressed and glued to the tape using cotton-tipped applicators. Alternatively, the liver itself may be glued directly to the coverglass along the periphery of the window. Sterile 0.9% saline is then placed in the coverslip-bottomed dish to keep liver moist throughout the imaging session. A small dose (0.2mg/kg) of sodium fluorescein (Fluka Analytical) is administered IV in order to generate dim labeling of bile canaliculi that can be used to facilitate positioning of the liver at the beginning of the study.

2.3 Multiphoton microscopy - The studies described here were conducted using two Olympus Fluoview 1000 microscope systems. Images shown in Figures 1, 2, 4, 7 and 8 were collected using an Olympus Fluoview 1000 MPE laser scanning confocal/multiphoton microscope system mounted to an IX81 inverted microscope stand, equipped with a Spectraphysics MaiTai DeepSee titanium sapphire laser (Spectraphysics, Santa Clara, CA). Fluorescence emissions were collected in three non-descanned photomultiplier detectors, with bandpass filters for blue (420-460 nm), green (495-540 nm) and red (570-630 nm) fluorescence emissions. The image shown in Figure 5 was collected using an Olympus Fluoview 1000 laser scanning confocal microscope system modified for multiphoton fluorescence excitation imaging. This system is mounted to an IX81 inverted microscope stand and is fitted with a Spectraphysics MaiTai titanium sapphire laser (Spectraphysics, Santa Clara, CA), a Pockels cell electro-optical attenuator (Conoptics Inc., Danbury, CT), and a Keplerian collimator/beam expander. Images are collected via a custom designed 3 channel external detector system equipped with gallium arsenide phosphide detectors (Hamamatsu, Hamamatsu City, Japan) with bandpass filters for blue (380-480 nm), green (500-550 nm) and red (560-650 nm) fluorescence emissions. Images were collected using IR-optimized water immersion objectives: either an Olympus 20X, NA 0.95 objective or an Olympus 25X, NA 1.05, objective.

Fluorescence excitation is accomplished using illumination wavelengths from 800-830 nm. Images are generally collected at a rate of approximately 1 frame per second at a frame size of 512 by 512 pixels. Zoom and focal plane spacing are typically set for a voxel size of 0.7 by 0.7 by 1 micron. Photomultiplier voltages are adjusted such that minimal laser power yields images with detectible fluorescence in the hepatocyte cytosol before addition of probe. A guiding principle in intravital microscopy is to limit the level of illumination in order to avoid photo-toxicity and photobleaching of fluorescent probes. For our studies, we typically evaluate the effect of imaging by comparing images of the field used to characterize kinetics with images of nearby fields for

evidence of damage (reduced microvascular flow, microvascular leakage, disrupted cell integrity) or photobleaching.

In order to ensure that measurements are comparable between different animals, replicate studies are conducted using the same objective lens and identical laser power and detector settings. Reproducible measurements of multiphoton-excited fluorescence additionally depend upon use of the same excitation wavelength and pulse duration. Insofar as signal levels in intravital microscopy also depend upon the depth at which images are collected in the tissue, all images are collected from the same depth in the tissue (typically 10-20 microns in our studies).

Quantitative measurements depend upon signal linearity. Detector offset should be adjusted to ensure collection of weak signals, and accurate estimation of background fluorescence. Illumination and detector gain must be adjusted such that the strongest signals are detected without saturating the detector. In practice, the dynamic range of laser scanning confocal/multiphoton microscope systems is such that it can be exceeded due to the enormous range of fluorescence intensities in different compartments over the course of a time-series. Nonetheless, accurate measurements of transport kinetics can typically be obtained as long as signal saturation is avoided during the initial intervals of hepatocyte uptake and secretion.

2.4 Fluorescent probes for intravital microscopy analyses of hepatic transport

2.4.1 - Fluorescent probes for analysis of organic anion transport - Fluorescein and its derivatives are the most commonly used fluorescent transport probes [31]. Fluorescein exhibits minimal toxicity (LD_{50} of 1 g/kg in rats) and fluorescein-based probes have been used in hepatic transport studies for more than 70 years [18-25, 27, 28]. Fluorescein is an organic anion substrate of the human and rat organic anion (OAT/Oat and OATP/Oatp) transporters [32] Human MRP2 [33, 34] that is rapidly glucuronidated in hepatocytes [35-37], making it an appropriate probe for MRP2- and MRP3-mediated anion glucuronate secretion.

Modified forms of fluorescein have also been widely used to study hepatic transport. Dichloro-fluorescein is also a substrate for rat Oatp, Mrp2 and Mrp3 [38], but we find that its utility *in vivo* is compromised by significant quenching of its fluorescence by constituents of the serum.

6-carboxyfluorescein diacetate (6-CFDA) is another fluorescent probe that has been widely used to evaluate transport *in vitro*, [39] and *in vivo* [27, 28]. As shown in **Figure 3A**, intravenous injection of 6-CFDA results in the rapid transport of the fluorescent probe into bile canaliculi within minutes of administration. 6-CFDA differs from fluorescein in that it is membrane permeant, but upon exposure to esterases becomes highly charged, so that while its uptake is passive, its secretion depends upon active transport, which is mediated by Mrp2 and Mrp3 in rat hepatocytes [38].

In studies of the in vivo effects of rifampin on hepatic transport, we attempted to exploit the membrane permeability of 6-CFDA to evaluate effects on the secretory pathway [22]. We had found that rifampin essentially blocked hepatic uptake of fluorescein confounding our ability to assess the effect of rifampin on hepatocyte secretory function. We anticipated that passive uptake would yield sufficient cytosolic delivery of 6-CFDA to support analysis of the effects of rifampin on secretion. However, we found that, like fluorescein, the

uptake of 6-CFDA was inhibited by rifampin. In retrospect, it is likely that this result reflects hydrolysis of the intravenously-delivered 6-CFDA in the blood to its membrane impermeant form. Previous studies demonstrated that esterases present in the blood rapidly hydrolyze Carboxy-Dichlorofluorescein Diacetate (CDFDA) [38] and various fluorescent probes containing acetoxy-methyl esters [40], eliminating their capacity for passive cell permeability *in vivo*. Thus, although 6-CFDA can be used to evaluate hepatic transport *in vivo*, it should be used with the understanding that hepatic uptake is likely to be at least partially mediated by active transport processes.

2.4.2 - Fluorescent probes for analysis of bile acid transport – Cholyl-lysl-fluorescein (CLF) is a fluorescein-labeled bile acid that has been previously used to evaluate hepatic transport in vitro [16, 41] and in vivo [42]. **Figure 3B** shows an image of the liver of a living rat 10 minutes after intravenous injection of CLF. Studies of Mrp2-deficient TR- rats suggest that hepatic secretion of CLF is independent of Mrp2 and is mediated by Bsep in rats [43, 44]. In contrast, studies of transfected cells suggest that CLF secretion is mediated by MRP2 rather than BSEP in humans [45].

Cholyl-glycyl-amido-fluorescein (CGamF), is a fluorescent bile acid whose transport, in a comparison with a variety of other fluorescent bile acids was found to most closely resemble native bile acids [46]. Hepatic uptake of CGamF is mediated by Ntcp/NTCP, but primarily by Oatps/OATP [47-50], while CGamF secretion is mediated by BSEP/Bsep [47, 51]. **Figure 3C** shows an example of an image that demonstrates the uptake and canalicular secretion of CGamF by hepatocytes in the liver of a living rat following intravenous injection.

2.4.3 - Additional fluorescent probes for in vivo studies of hepatic transport – Although the preponderance of intravital microscopy studies of hepatic transport utilize fluorescein or a derivative, the reader is also referred to additional probes have been used for *in vivo* studies, including the long wavelength dyes DY635 and indocyanine green [26, 52], NBD-conjugates of bile acids [46, 53] and rhodamine-123 [54].

Most epifluorescence systems (wide-field, confocal or two-photon excitation) are designed to collect multiple colors of fluorescence, supporting simultaneous characterizations of multiple properties. So, for example, fluorescent dextrans can be used alongside fluorescent transport substrate to characterize microvascular function [27, 28, 55]. Throughout this review we show how Hoechst 33342 can be used to label nuclei, providing spatial cues for identifying and distinguishing cells. In previous studies, we have shown that Hoechst can also be used to identify apoptotic cells, which are apparent on the basis of their condensed/fragmented nuclei [30, 56]. **Figure 3D** shows an how propidium iodide, a membrane-impermeant, DNA-binding probe can be used to identify necrotic hepatocytes in a field of the liver collected from a rat 3 hrs after treatment with acetaminophen. The close proximity of the patch of necrotic cells alongside fields of healthy hepatocytes actively transporting fluorescein highlights the focal nature of acetaminophen-induced liver injury.

2.5 Intravital microscopy imaging procedures - The microscope stage is warmed with heating pads, and the objective lens is heated with an objective heater. The rat is placed ventral side down on the stage of an

inverted microscope and the attached coverslip-bottom dish is inserted into the 50 mm stage aperture and taped in place. A second heating pad is then placed over the rat. The hind legs of the rat are then taped securely to prevent movement. A schematic diagram of the arrangement of the rat on the microscope stage is shown in **Figure 4**. The depth of anesthesia is monitored by visual inspection of respiration and core temperature is monitored via rectal thermometer. Blood pressure can be monitored via a transducer attached to a femoral artery catheter.

Using wide-field epifluorescence viewed through the microscope eyepiece, an appropriate field, focused to a depth of the first layer of hepatocytes is identified using the dim fluorescence of the fluorescein-labeled canaliculi. Microvascular flow is also apparent in epifluorescence, and is used to ensure that the blood flow to the liver has been maintained during preparation for imaging. The field is then scanned using laser scanning multiphoton excitation to identify the top and bottom of a 6 micron deep volume that incorporates an extensive network of sinusoids and canaliculi (such as that shown in Figure 2). Using these settings, a series of 3D image volumes (6 focal planes, spaced 1 micron apart) are then collected continuously just before and for ten minutes following injection of a fluorescent probe. Unrestricted blood flow, apparent in the rapid movement of the shadows of blood cells through the sinusoids is monitored throughout the interval. In order to minimally increase blood volume, probes are introduced in minimal volumes, typically to a total of 0.4 ml.

2.6 Digital image analysis - Quantitative data are derived from the time-series images using methods of digital image analysis. The methods described below were developed using Metamorph image processing software (Molecular Devices, Downington, PA), but are based upon simple tools available in other image processing packages.

2.6.1 - Production of extended depth images - projection of image volumes – The kinetics of probe transport are captured as a time-series of 3D volumes, rather than a series of images of single planes. This approach is taken to minimize the effects of motion on quantitative analyses. The quantitative assays described below depend upon measuring changes in fluorescence occurring in subcellular compartments that are separated by fractions of a micron. In order to make measurements of each of these compartments over time, the field must thus be immobilized to subcellular precision. While sample stability is easily accomplished in studies of cultured cells, it is more challenging in studies of cells in living animals, particularly for the liver, since it is located immediately below the diaphragm.

Much of the respiration-induced motion is eliminated by tethering the liver to the coverslip-bottomed dish (as described above). The elimination of horizontal motion is demonstrated in **Figure 5**, which shows the results of a study in which 139 sequential images of nuclei were collected from a single image plane in the liver of a living rat. The absence of horizontal motion is apparent in the sharp appearance of the nuclei in the maximum projection of the entire series of images shown in Panel A, but is especially obvious in Panel B, which shows an XT projection of the region indicated in the red box. This image demonstrates that the sample has been immobilized to essentially single pixel lateral stability (0.7 microns).

However, examination of the XT projection shows that there are gaps where nuclei disappear from the time series. These gaps reflect vertical motion of the tissue sufficient to move the nuclei beyond the focal plane. In order to accommodate this residual vertical motion, we effectively capture a larger focal volume by collecting each time point as a 3D volume. Each of these 3D volumes is then converted into a single, extended-focus image by maximum-projection. We find that this approach ensures that the structure of the canaliculi and sinusoids are more consistently captured, regardless of small vertical translations in the tissue. The effectiveness of this approach for quantitative studies is demonstrated in **Figure 6**, which shows that the wild variability obtained from an analysis of a time series of single images (Panel C) is substantially reduced in measurements obtained from time series of the projected image volumes (Panel D).

This approach also has the effect of capturing more of the canalicular network in the field; whereas the canaliculi are fragmented in the image of a single focal plane (Panel A), the canalicular network is much more complete in the maximum projection of 6 focal planes. The effectiveness of this approach for maintaining the canalicular network in the field of view throughout the time series is also demonstrated in **Video 2**.

2.6.2 - Quantitative analysis of transport via measurements of regions-of-interest drawn in individual cells – As mentioned above, we quantify hepatocyte transport *in vivo* by quantifying changes in the fluorescence of the cytosol and bile canaliculi in image volume projections collected from the liver over time after intravenous injection of a fluorescent transport substrate.

One approach is to measure changes in mean fluorescence in regions of interest that are manually drawn over the cytosol and bile canaliculi of individual cells [22, 23]. The mean fluorescence in each region is then automatically measured for each image in the time series, producing a series of values reflecting the kinetics of probe fluorescence changes in the compartment. Using this approach, the rate of hepatocyte uptake is measured as the initial linear rate of increase in fluorescence in regions of interest measured in the cytosol of 20-50 hepatocytes (typically during the first 30 seconds after perfusion). The rate of canalicular secretion is measured in regions of interest located over the canaliculi of the same hepatocytes (typically during the period from 30 seconds to 2 minutes after perfusion). Signal linearity is established by (1) verifying that intensity measurements do not exceed detector saturation and (2) subtracting the mean fluorescence measurements obtained prior to perfusion from all measurements.

Quantitative analyses of the image series shown in Video 1 are shown in **Figure 7**. Rate calculations demonstrate that treatment with the cholestatic agent taurolithocholate reduces the rate of fluorescein uptake by nearly 60% and the rate of fluorescein secretion by more than 50%. These results suggest that TLC inhibits both uptake and secretion, however the effect on secretion is less obvious when one considers the lower amount of fluorescein in the cytosol of hepatocytes of the TLC-treated rat. Insofar as the rate at which fluorescein appears in the canaliculi depends upon the concentration of fluorescein in the cytosol, we may want to measure secretion in terms of “specific secretion”, in which the raw rate of secretion is divided by the mean cytosolic fluorescence. Measured in this way, the effect of TLC is much less obvious, reducing the rate of specific secretion by only ~10%.

Insofar as kinetics are measured in terms of changes in detected fluorescence, reproducibility between measurements made in different animals depends upon fastidious maintenance of imaging conditions. All imaging must be conducted with identical plasma concentrations of fluorescein, at the same depth into the liver at identical levels of illumination, and with identical photomultiplier settings. Despite unavoidable variability in each of these parameters, reproducibility in these transport assays is high. We previously found that a sample size of 5 rats was sufficient to detect a 20% decrease in the rate of hepatic uptake of fluorescein in an experimental model of chronic kidney disease [23].

2.6.3 - Quantitative analysis of field-wise transport via automatically-generated regions of interest – The method described above is based upon characterizing a sample of cells that are deemed representative of the field, if not the liver. In this regard, this approach is effective for evaluating the effects of experimental manipulations that have a relatively consistent effect on all of the hepatocytes in a field. To the degree that responses vary between cells, the validity of this method is susceptible to sampling error. An example of a heterogeneous response is shown in **Video 3**, which shows that canalicular transport is blocked in most, but not all of the hepatocytes in a field collected from a rat 2 hrs after IV injection of 4 mg/kg endotoxin. While a cell-by-cell analysis might yield interesting insights as to focal effects of endotoxin, for example as a function of position in a lobule, it would be difficult to design a cell sampling approach that would support estimation of the overall effect on the entire field. To facilitate simple, bias-free measurements of the response of an entire field, we developed techniques for measuring hepatocyte uptake and secretion using automatically identified regions-of-interest for the cytosol and canaliculi.

Field-wise canalicular transport is quantified as the change in the integrated fluorescence of the green channel in automatically-generated masked regions generated using a high-pass spatial filter. The approach is predicated on the fact that canaliculi appear as narrow structures that are detectibly brighter than the surrounding cytosol. Since Hoechst fluorescence bleeds into the green channel on our systems, each of the projected images of the green channel is first crosstalk-corrected by subtraction of the corresponding image of the blue channel. A high-pass filtered image is then obtained by subtraction of a large-neighborhood median-filtered image [57]. The final canalicular mask is obtained by elimination of single pixels from the high-pass-filtered image. The effectiveness of this approach for automatically delineating the region of bile canaliculi is demonstrated in **Figure 8** and **Video 4**.

A time series of masks is generated and canalicular fluorescence for each time point is quantified as the integrated signal of the green channel occurring within the masked region. Measurements are corrected for background by subtracting the mean signal measured prior to introduction of the fluorescent probe. As described above, canalicular secretion rate is quantified as the linear slope during initial interval of canalicular accumulation (typically 1 minute after infusion, ~2 minutes after injection).

Field-wise cytosolic transport is quantified as the change in mean green-channel fluorescence in a set of automatically generated regions-of-interest in the cytosol of hepatocytes, defined as 2 pixel wide regions 6 pixels away from the boundary of the nuclei. Masks of the nuclei in each projected image are first created by thresholding images of the blue channel, which contains images of Hoechst-labeled nuclei. Cytosolic regions-

of-interest are generated by dilating the objects in the binarized image of the nuclei 8 times and then subtracting the resulting mask from a binary mask of the image created by dilating 6 times (in each case, using a neighborhood of 3). Overlap of canaliculi with the cytosolic regions-of-interest is eliminated by subtracting the corresponding canalicular mask from each. Examples of representative cytosolic regions-of-interest are shown in **Figure 8**. Cytosolic fluorescence for each time point is quantified as the mean green channel signal occurring in the cytosolic regions-of-interest, after subtraction of the mean integrated signal measured prior to introduction of the fluorescent probe. Cytosolic uptake rate is quantified as the linear slope during initial interval of cytosolic uptake accumulation (starting immediately upon infusion, typically 1 minute after injection).

This automated approach for identifying the canalicular and cytosolic regions offers several advantages over the single-cell analysis procedure. First, the automated approach provides measures of field-wise responses that are less susceptible to bias, since it does not depend upon operator identifying cells and regions for quantification. Second, the automated procedure requires significantly less time and effort than the single cell approach, which requires manually drawing regions of interest. Finally, it is less sensitive to motion artifacts. Insofar as the manual technique utilizes a single mask of the regions-of-interest, accurate measurements depend upon the continuous alignment of the images with the single region mask throughout the time series. In contrast, the automated approach generates regions-of-interest from each image in the time series, and so is insensitive to lateral motion in the field.

An example of a field-wise analysis of hepatic transport is shown in **Figure 9**, which summarizes the effects of endotoxin on fluorescein transport in rats. Figure 9A shows a projected image of a field collected from the liver of a rat 1 hour after intraperitoneal injection of 4 mg/kg bacterial endotoxin. When compared with the comparable image collected from a control animal (Figure 1), this image clearly demonstrates how endotoxin treatment induces an accumulation of fluorescein in the cytosol of hepatocytes. The overall effects of endotoxin are also dramatically demonstrated in Video 3, which shows a comparison of fluorescein transport by a control rat and a rat 2 hours after endotoxin treatment.

The quantitative analysis of field-wise canalicular fluorescence shown in Figure 9B demonstrates that fluorescein secretion is completely blocked 1 hour after treatment with endotoxin, and is only beginning to recover by 2 hours. This result is consistent with *in vivo* studies of rats and *ex vivo* studies of human liver slices demonstrating that endotoxins induce a rapid internalization of three major canalicular transporters Mrp2, Bsep and aquaporin8, resulting in decreased bile secretion [58-63].

The analysis of cytosolic fluorescence shown in Figure 9C demonstrates that the rate of fluorescein uptake is essentially unaffected by endotoxin so that, in the absence of canalicular secretion, fluorescein accumulates to cytosolic concentrations increase 2-3 fold over those in the control rat.

Figure 10 shows the results of a similar analysis of the effects of TLC on hepatic transport of the fluorescent bile acid CGamF. Quantitative analysis of field-wise measurements demonstrate that TLC reduces the rate of CGamF secretion by 8 fold (Figure 10A), while having no effect on the rate of uptake (Figure 10B). As found in rats treated with endotoxin, unabated uptake in the absence of secretion leads to a protracted accumulation of CGamF in the hepatocyte cytosols of TLC treated rats.

3. Conclusions

These studies demonstrate that the speed and resolution of quantitative intravital microscopy can be used to provide unique insights into the mechanism and consequences of cholestasis *in vivo*. The complexity of hepatic transport, which for any given substrate involves multiple transporters, each of which is physiologically regulated, makes it difficult to predict *in vivo* effects from results obtained from *in vitro* studies. Extrapolating the *in vivo* effects of a drug from *in vitro* data is further complicated by the complexity of factors determining local *in vivo* drug exposures. Quantitative intravital microscopy provides a direct window into the realized, *in vivo* effects of a drug, integrated across all of these variables.

In addition to identifying net effects, intravital microscopy is also uniquely capable of distinguishing acute effects on uptake and secretion, and determining whether transport is disrupted in such a way as to increase the cytosolic concentration of transport substrates. The ability to detect acute effects on the cytosolic load of transport substrates may be particularly useful in that the cytosolic accumulation of drugs and/or toxic metabolites is believed to mediate the hepatotoxicity of many drugs associated with drug-induced liver injury [1-3]. The relationship between cytosolic substrate accumulation and cytotoxicity is complicated by the fact that the adaptive changes in transporter expression made by hepatocytes during cholestasis are also believed to be mediated by the cytosolic accumulation of bile acids [12, 64-66].

4. Challenges and outlook

4.1 - Microscopy provides a small window – can observations be extrapolated to the entire organ? - Intravital microscopy provides a high-resolution window into hepatic transport, but the window is small; our studies of transport kinetics are conducted using 20-25X objectives, providing a field of view less than 400 microns across. To some degree, one can validate observations made in a small field by collecting data from multiple fields, but the kinetics of probe clearance are such that it is difficult to collect kinetic data for more than 2-3 fields from a single animal. One can also build a larger-scale mosaic from images collected from contiguous regions (i.e. Figure 1). However, these mosaics take tens-of-minutes to collect and so, while they can be useful for characterizing spatial heterogeneity in probe transport, they cannot provide kinetic data at the timescale of hepatic transport.

The obvious solution would be to image at lower magnification; a 2.5X objective could be used to image an area 100x larger than a 25X objective. The problem is that, for conventional objective lenses, low power objectives necessarily also have low numerical apertures, compromising resolution and light collection efficiency. Alternative light-collection schemes have been developed to increase the efficiency of light collection in multiphoton microscopy [67, 68], however these do not improve the problem of resolution. A 2.5X objective with numerical aperture of .07 will provide lateral resolution around 4-fold too low to resolve bile canaliculi. New scanner and lens designs have recently been developed that provide sub-micron resolution over 5-6 mm fields [69, 70] but, at the time of writing, these systems are not commercially available.

The window into the liver is also very shallow; our studies are typically conducted at depths of only 10-20 microns into the liver. Insofar as the reach of light microscopy is limited by scattering and refractive index

discontinuities, it may be increased by using longer wavelengths of light [71] and/or using beam shaping approaches such as adaptive optics [72], respectively.

However, these improvements need to be put in perspective – at best they may increase our field of view from the scale of microns to the scale of millimeters, still laughably small relative to the total volume of a single lobe, much less the entire liver. In the end, intravital microscopy studies should be complemented with conventional approaches. While conventional analyses of blood and bile samples cannot reproduce, much less validate measures of subcellular kinetics, they can provide complementary evidence that they are representative [24]

4.2 - Effects of intravital microscopy on liver function – have we perturbed the system we're evaluating? - The rationale for intravital microscopy is that it provides access to the behaviors of cells in the complete, relevant context of the intact living animal. However, the procedures involved in intravital microscopy are, to varying degrees, invasive and thus can perturb normal function. As described here and in other articles in this volume, investigators make every effort to ensure the physiological condition of animals on the microscope stage.

One concession that most investigators make is to use general anesthetics, which themselves can affect hepatic transport [73, 74] and potentially introduce drug-drug interactions that complicate studies. Anesthesia is necessary for imaging animals using conventional microscope systems, but miniaturized microscopes have been developed that can be mounted on the skull or back, to support imaging of physiology in non-anesthetized "awake" animals [75, 76]. While "miniaturized", current systems remain too bulky for imaging visceral organs in freely-moving animals.

Our studies utilize animals whose livers are imaged within minutes of surgical exposure. In order to avoid collecting data immediately following the trauma of surgery, imaging can be delayed through the use of a window chamber that can be implanted the day before [28]. Similar windows have been refined to the point that they can be used to repeatedly image tissues over periods of weeks, supporting powerful longitudinal studies [77]. Windows of this kind are described in detail in another article in this issue.

4.3 - Building quantitative models from data obtained from intravital microscopy studies - The utility of quantitative fluorescence microscopy for studies of hepatic transport is based upon a few critical assumptions. First, it depends upon the validity of using fluorescent probes as proxies for molecules of interest (drugs, bile acids). As described in section 2.4, there are multiple fluorescent probes that have been validated as substrates for the transporters involved in hepatic transport.

Second, fluorescence microscopy assays of transport kinetics depend upon the assumption that measurements reflect probe concentrations. In fact, measured fluorescence is a function not only of concentration, but also of the efficiency with which fluorescence is stimulated and collected, and the linearity with which collected fluorescence is converted into a digital signal. These issues can be addressed through a thoughtful and consistent approach to imaging, as described in Section 2.3. However, the relationship between fluorescence and concentration is complicated by the fact that probe fluorescence is reduced by

binding to proteins and, in the case of fluorescein, from enzymatic modification to fluorescein glucuronide, which profoundly reduces fluorescence [35, 46]. Thus, even if one were to calibrate fluorescence measurements to account for differences in the illumination and fluorescence detection, it is not possible to assign a concentration to a fluorescence measurement without a complete understanding of the degree to which fluorescein's fluorescence is quenched in different compartments at different times.

A promising approach to measuring fluorescence quenching *in vivo* is to complement measures of fluorescence intensity with measures of fluorescence lifetime, which decreases proportionally with quenching. The Roberts lab has pioneered the use of intravital fluorescence lifetime microscopy of the liver [21, 24, 25, 78]. Recently-developed systems supporting rapid measurement of fluorescence lifetime may make it possible to sensitively measure the kinetics of fluorescence intensity and fluorescence lifetimes in the blood, hepatocyte cytosol and canaliculi *in vivo*. To the degree that fluorescence lifetimes can be used to estimate quenching, this approach could be used to translate measures of intensity into measures of probe concentration in each compartment over time and thus to estimate transport parameters based upon Michaelis-Menten kinetics. These kinetic parameters could be compared directly with results obtained from *in vitro* studies, for example to estimate local *in vivo* drug concentrations. These parameters could also be used to populate models of in vivo transport that could identify effects on transport pathways that cannot be directly evaluated, for example, transport from hepatocytes back into the sinusoids.

4.4 - Clinical application of intravital microscopy for studies of hepatic function - Generally an invasive procedure, high-resolution intravital microscopy is almost exclusively conducted in studies of animal models. However, the approaches described here are remarkably compatible with clinical application. First, both fluorescein and indocyanine green are approved for use in human studies. Second, the surface of the liver can be accessed via laparoscopy, a procedure in which imaging is conducted using a narrow probe inserted through a minor incision in the abdomen.

The feasibility of fluorescence laparoscopy as an approach for evaluating hepatic function was demonstrated nearly 30 years ago in studies in which a wide-field epifluorescence probe was used to image fluorescein in the liver of humans and rats [79]. The approach has since been refined with the development of a confocal endo-microscope that provides resolution sufficient to distinguish sinusoids, hepatocytes and canaliculi in humans following intravenous injection of fluorescein [80]. Using systems of this kind, assays of liver function, developed in intravital microscopy studies of animal models, may find clinical application as a means to understand cholestasis and perhaps predict cholestatic liver injury.

Acknowledgments

This work was supported by the National Institutes of Health O'Brien Center for Advanced Renal Microscopic Analysis (NIH-NIDDK P30DK079312). Microscopy studies were conducted at the Indiana Center for Biological Microscopy. I thank Jennifer Ryan, Clifford Babbey, Marwan Ghabril, Erin Gill, Henry Mang and George Rhodes for contributions to the development of the techniques described here.

Table 1 – Commercially available probes used for intravital studies of hepatic transport

Transport assay	Probe	Dose	Vendor	Reference
Organic anion uptake and secretion	Sodium fluorescein	2 mg/kg	Sigma Aldrich (St. Louis, MO, USA)	[18-25, 27]
	Indocyanine green	10 µg/kg	Pulsion Medical Systems SE (Feldkirchen, Germany)	[26, 52]
	Rhodamine-123	2 mg/kg	Sigma Aldrich (St. Louis, MO, USA)	[54]
	DY635	10 µg/kg	Dyomics GmBH (Jena, Germany)	[26, 52]
Organic anion secretion	6-Carboxyfluorescein diacetate	0.2 mg/kg	Sigma Aldrich (St. Louis, MO, USA)	[22, 27, 28]
Bile acid uptake and secretion	Cholyl-lysl-fluorescein	0.5 mg/kg	Syncon (Groningen, Netherlands)	[42-44]
	Cholyl-glycyl-amido-fluorescein	0.4 mg/kg	WuXi AppTec (Tianjin, China)	This chapter

References

1. Morgan, R.E., et al., *Interference with bile salt export pump function is a susceptibility factor for human liver injury in drug development.* Toxicol Sci, 2010. **118**(2): p. 485-500.
2. Dawson, S., et al., *In vitro inhibition of the bile salt export pump correlates with risk of cholestatic drug-induced liver injury in humans.* Drug Metab Dispos, 2012. **40**(1): p. 130-8.
3. Kostrubsky, V.E., et al., *Evaluation of hepatotoxic potential of drugs by inhibition of bile-acid transport in cultured primary human hepatocytes and intact rats.* Toxicol Sci, 2003. **76**(1): p. 220-8.
4. Donner, M.G. and D. Keppler, *Up-regulation of basolateral multidrug resistance protein 3 (Mrp3) in cholestatic rat liver.* Hepatology, 2001. **34**(2): p. 351-9.
5. Paulusma, C.C., et al., *Zonal down-regulation and redistribution of the multidrug resistance protein 2 during bile duct ligation in rat liver.* Hepatology, 2000. **31**(3): p. 684-93.
6. Donner, M.G., et al., *Enhanced expression of basolateral multidrug resistance protein isoforms Mrp3 and Mrp5 in rat liver by LPS.* Biol Chem, 2004. **385**(3-4): p. 331-9.
7. van de Steeg, E., et al., *Complete OATP1B1 and OATP1B3 deficiency causes human Rotor syndrome by interrupting conjugated bilirubin reuptake into the liver.* J Clin Invest, 2012. **122**(2): p. 519-28.
8. van de Steeg, E., et al., *Organic anion transporting polypeptide 1a/1b-knockout mice provide insights into hepatic handling of bilirubin, bile acids, and drugs.* J Clin Invest, 2010. **120**(8): p. 2942-52.
9. Roma, M.G., F.A. Crocenzi, and A.D. Mottino, *Dynamic localization of hepatocellular transporters in health and disease.* World J Gastroenterol, 2008. **14**(44): p. 6786-801.
10. Crocenzi, F.A., et al., *Localization status of hepatocellular transporters in cholestasis.* Front Biosci, 2012. **17**: p. 1201-18.
11. Zollner, G., M. Wagner, and M. Trauner, *Nuclear receptors as drug targets in cholestasis and drug-induced hepatotoxicity.* Pharmacol Ther, 2010. **126**(3): p. 228-43.
12. Wagner, M., G. Zollner, and M. Trauner, *Nuclear receptor regulation of the adaptive response of bile acid transporters in cholestasis.* Semin Liver Dis, 2010. **30**(2): p. 160-77.
13. Mottino, A.D. and V.A. Catania, *Hepatic drug transporters and nuclear receptors: regulation by therapeutic agents.* World J Gastroenterol, 2008. **14**(46): p. 7068-74.
14. Barth, C.A. and L.R. Schwarz, *Transcellular transport of fluorescein in hepatocyte monolayers: evidence for functional polarity of cells in culture.* Proc Natl Acad Sci U S A, 1982. **79**(16): p. 4985-7.
15. Gebhardt, R. and W. Jung, *Biliary secretion of sodium fluorescein in primary monolayer cultures of adult rat hepatocytes and its stimulation by nicotinamide.* J Cell Sci, 1982. **56**: p. 233-44.
16. Swift, B., N.D. Pfeifer, and K.L. Brouwer, *Sandwich-cultured hepatocytes: an in vitro model to evaluate hepatobiliary transporter-based drug interactions and hepatotoxicity.* Drug Metab Rev, 2010. **42**(3): p. 446-71.
17. Kitamura, T., Z. Gatmaitan, and I.M. Arias, *Serial quantitative image analysis and confocal microscopy of hepatic uptake, intracellular distribution and biliary secretion of a fluorescent bile acid analog in rat hepatocyte doublets.* Hepatology, 1990. **12**(6): p. 1358-64.
18. Hanzon, V., *Liver cell secretion under normal and pathologic conditions studied by fluorescence microscopy on living rats.* Acta Physiol Scand Suppl, 1952. **28**(101): p. 1-268.
19. Sherman, I.A. and M.M. Fisher, *Hepatic transport of fluorescent molecules: in vivo studies using intravital TV microscopy.* Hepatology, 1986. **6**(3): p. 444-9.
20. Watanabe, N., et al., *Motility of bile canaliculi in the living animal: implications for bile flow.* J Cell Biol, 1991. **113**(5): p. 1069-80.
21. Roberts, M.S., et al., *In vitro and in vivo imaging of xenobiotic transport in human skin and in the rat liver.* J Biophotonics, 2008. **1**(6): p. 478-93.
22. Babbey, C.M., et al., *Quantitative intravital microscopy of hepatic transport.* Intravital, 2012. **1**(1): p. 10.
23. Ryan, J.C., K.W. Dunn, and B.S. Decker, *Effects of chronic kidney disease on liver transport: quantitative intravital microscopy of fluorescein transport in the rat liver.* Am J Physiol Regul Integr Comp Physiol, 2014. **307**(12): p. R1488-92.
24. Thorling, C.A., et al., *Assessing steatotic liver function after ischemia-reperfusion injury by in vivo multiphoton imaging of fluorescein disposition.* Drug Metab Dispos, 2015. **43**(1): p. 154-62.
25. Thorling, C.A., et al., *Intravital multiphoton microscopy can model uptake and excretion of fluorescein in hepatic ischemia-reperfusion injury.* J Biomed Opt, 2013. **18**(10): p. 101306.
26. Gonnert, F.A., et al., *Hepatic excretory function in sepsis: implications from biophotonic analysis of transcellular xenobiotic transport in a rodent model.* Crit Care, 2013. **17**(2): p. R67.

27. Liu, Y., et al., *Visualization of hepatobiliary excretory function by intravital multiphoton microscopy.* J Biomed Opt, 2007. **12**(1): p. 014014.
28. Li, F.C., et al., *In vivo dynamic metabolic imaging of obstructive cholestasis in mice.* Am J Physiol Gastrointest Liver Physiol, 2009. **296**(5): p. G1091-7.
29. National Research Council (U.S.). Committee for the Update of the Guide for the Care and Use of Laboratory Animals., Institute for Laboratory Animal Research (U.S.), and National Academies Press (U.S.), *Guide for the care and use of laboratory animals*. 2011, National Academies Press,: Washington, D.C. p. xxv, 220 p.
30. Dunn, K.W., et al., *Functional studies of the kidney of living animals using multicolor two-photon microscopy.* Am J Physiol Cell Physiol, 2002. **283**(3): p. C905-16.
31. Robertson, T.A., F. Bunel, and M.S. Roberts, *Fluorescein derivatives in intravital fluorescence imaging.* Cells, 2013. **2**(3): p. 591-606.
32. De Bruyn, T., et al., *Sodium fluorescein is a probe substrate for hepatic drug transport mediated by OATP1B1 and OATP1B3.* J Pharm Sci, 2011. **100**(11): p. 5018-30.
33. Mor-Cohen, R., et al., *Identification and functional analysis of two novel mutations in the multidrug resistance protein 2 gene in Israeli patients with Dubin-Johnson syndrome.* J Biol Chem, 2001. **276**(40): p. 36923-30.
34. van der Kolk, D.M., et al., *Activity and expression of the multidrug resistance proteins MRP1 and MRP2 in acute myeloid leukemia cells, tumor cell lines, and normal hematopoietic CD34+ peripheral blood cells.* Clin Cancer Res, 1998. **4**(7): p. 1727-36.
35. Blair, N.P., et al., *Fluorescein and fluorescein glucuronide pharmacokinetics after intravenous injection.* Invest Ophthalmol Vis Sci, 1986. **27**(7): p. 1107-14.
36. Chahal, P.S., M.J. Neal, and E.M. Kohner, *Metabolism of fluorescein after intravenous administration.* Invest Ophthalmol Vis Sci, 1985. **26**(5): p. 764-8.
37. Webb, J.M., M. Fonda, and E.A. Brouwer, *Metabolism and excretion patterns of fluorescein and certain halogenated fluorescein dyes in rats.* J Pharmacol Exp Ther, 1962. **137**: p. 141-7.
38. Zamek-Gliszczynski, M.J., et al., *Pharmacokinetics of 5 (and 6)-carboxy-2',7'-dichlorofluorescein and its diacetate promoiety in the liver.* J Pharmacol Exp Ther, 2003. **304**(2): p. 801-9.
39. Nakanishi, T., et al., *Quantitative time-lapse imaging-based analysis of drug-drug interaction mediated by hepatobiliary transporter, multidrug resistance-associated protein 2, in sandwich-cultured rat hepatocytes.* Drug Metab Dispos, 2011. **39**(6): p. 984-91.
40. Jobsis, P.D., E.C. Rothstein, and R.S. Balaban, *Limited utility of acetoxymethyl (AM)-based intracellular delivery systems, in vivo: interference by extracellular esterases.* J Microsc, 2007. **226**(Pt 1): p. 74-81.
41. Letzsch, S., et al., *Quantifying Efflux Activity in 3D Liver Spheroids.* Genetic Engineering and Biotechnology News, 2015. **35**(7): p. 2.
42. Milkiewicz, P., et al., *Visualization of the transport of primary and secondary bile acids across liver tissue in rats: in vivo study with fluorescent bile acids.* J Hepatol, 2001. **34**(1): p. 4-10.
43. Mills, C.O., et al., *Different pathways of canalicular secretion of sulfated and non-sulfated fluorescent bile acids: a study in isolated hepatocyte couplets and TR- rats.* J Hepatol, 1999. **31**(4): p. 678-84.
44. Mills, C.O., et al., *Cholyllysyl fluroscein and related lysyl fluorescein conjugated bile acid analogues.* Yale J Biol Med, 1997. **70**(4): p. 447-57.
45. de Waart, D.R., et al., *Hepatic transport mechanisms of cholyl-L-lysyl-fluorescein.* J Pharmacol Exp Ther, 2010. **334**(1): p. 78-86.
46. Holzinger, F., et al., *Fluorescent bile acid derivatives: relationship between chemical structure and hepatic and intestinal transport in the rat.* Hepatology, 1997. **26**(5): p. 1263-71.
47. Mita, S., et al., *Inhibition of bile acid transport across Na+/taurocholate cotransporting polypeptide (SLC10A1) and bile salt export pump (ABCB 11)-coexpressing LLC-PK1 cells by cholestasis-inducing drugs.* Drug Metab Dispos, 2006. **34**(9): p. 1575-81.
48. Ye, Z.W., P. Augustijns, and P. Annaert, *Cellular accumulation of cholyl-glycylamido-fluorescein in sandwich-cultured rat hepatocytes: kinetic characterization, transport mechanisms, and effect of human immunodeficiency virus protease inhibitors.* Drug Metab Dispos, 2008. **36**(7): p. 1315-21.
49. Ye, Z.W., et al., *Species-specific interaction of HIV protease inhibitors with accumulation of cholyl-glycylamido-fluorescein (CGamF) in sandwich-cultured hepatocytes.* J Pharm Sci, 2010. **99**(6): p. 2886-98.
50. Annaert, P., et al., *Interaction of HIV protease inhibitors with OATP1B1, 1B3, and 2B1.* Xenobiotica, 2010. **40**(3): p. 163-76.

51. Kruglov, E.A., et al., *Type 2 inositol 1,4,5-trisphosphate receptor modulates bile salt export pump activity in rat hepatocytes.* Hepatology, 2011. **54**(5): p. 1790-9.
52. Recknagel, P., et al., *In vivo imaging of hepatic excretory function in the rat by fluorescence microscopy.* J Biophotonics, 2012. **5**(7): p. 571-81.
53. Schramm, U., et al., *Fluorescent derivatives of bile salts. II. Suitability of NBD-amino derivatives of bile salts for the study of biological transport.* J Lipid Res, 1991. **32**(11): p. 1769-79.
54. Liu, X., Thorling, C., Jin, L. and M. Roberts, *Intravital multiphoton imaging of rhodamine 123 in the rat liver after intravenous dosing.* Intravital, 2012. **1**(1): p. 6.
55. Li, F.C., et al., *Apical membrane rupture and backward bile flooding in acetaminophen-induced hepatocyte necrosis.* Cell Death Dis, 2011. **2**: p. e183.
56. Kelly, K.J., et al., *A novel method to determine specificity and sensitivity of the TUNEL reaction in the quantitation of apoptosis.* Am J Physiol Cell Physiol, 2003. **284**(5): p. C1309-18.
57. Maxfield, F.R. and K.W. Dunn, *Studies of endocytosis using image intensification fluorescence microscopy and digital image analysis*, in *Optical Microscopy for Biology*, B.H.a.K. Jacobsen, Editor. 1990, Alan Liss: New York. p. 357-371.
58. Dombrowski, F., et al., *Electron-microscopic demonstration of multidrug resistance protein 2 (Mrp2) retrieval from the canalicular membrane in response to hyperosmolarity and lipopolysaccharide.* Biochem J, 2000. **348 Pt 1**: p. 183-8.
59. Elferink, M.G., et al., *LPS-induced downregulation of MRP2 and BSEP in human liver is due to a posttranscriptional process.* Am J Physiol Gastrointest Liver Physiol, 2004. **287**(5): p. G1008-16.
60. Kubitz, R., et al., *Regulation of the multidrug resistance protein 2 in the rat liver by lipopolysaccharide and dexamethasone.* Gastroenterology, 1999. **116**(2): p. 401-10.
61. Lehmann, G.L., et al., *LPS induces the TNF-alpha-mediated downregulation of rat liver aquaporin-8: role in sepsis-associated cholestasis.* Am J Physiol Gastrointest Liver Physiol, 2008. **294**(2): p. G567-75.
62. Sekine, S., et al., *Oxidative stress is a triggering factor for LPS-induced Mrp2 internalization in the cryopreserved rat and human liver slices.* Biochem Biophys Res Commun, 2010. **399**(2): p. 279-85.
63. Yano, K., et al., *The effect of dimerumic acid on LPS-induced downregulation of Mrp2 in the rat.* Biochem Pharmacol, 2010. **80**(4): p. 533-9.
64. Geier, A., et al., *Principles of hepatic organic anion transporter regulation during cholestasis, inflammation and liver regeneration.* Biochim Biophys Acta, 2007. **1773**(3): p. 283-308.
65. Klaassen, C.D. and L.M. Aleksunes, *Xenobiotic, bile acid, and cholesterol transporters: function and regulation.* Pharmacol Rev, 2010. **62**(1): p. 1-96.
66. Roma, M.G., F.A. Crocenzi, and E.A. Sanchez Pozzi, *Hepatocellular transport in acquired cholestasis: new insights into functional, regulatory and therapeutic aspects.* Clin Sci (Lond), 2008. **114**(9): p. 567-88.
67. McMullen, J.D., et al., *Enhancing collection efficiency in large field of view multiphoton microscopy.* J Microsc, 2011. **241**(2): p. 119-24.
68. Combs, C.A., et al., *Optimization of multiphoton excitation microscopy by total emission detection using a parabolic light reflector.* J Microsc, 2007. **228**(Pt 3): p. 330-7.
69. Sofroniew, N.J., et al., *A large field of view two-photon mesoscope with subcellular resolution for in vivo imaging.* Elife, 2016. **5**.
70. McConnell, G., et al., *A novel optical microscope for imaging large embryos and tissue volumes with sub-cellular resolution throughout.* Elife, 2016. **5**.
71. Andresen, V., et al., *Infrared multiphoton microscopy: subcellular-resolved deep tissue imaging.* Curr Opin Biotechnol, 2009. **20**(1): p. 54-62.
72. Booth, M.J., *Adaptive optics in microscopy.* Philos Trans A Math Phys Eng Sci, 2007. **365**(1861): p. 2829-43.
73. Collado, P.S., et al., *Effect of pentobarbital or urethane on bile secretion and chemical composition of blood in the rabbit.* Lab Anim, 1987. **21**(1): p. 11-7.
74. Mills, C.O., et al., *Effect of anaesthetic agents on bile flow and biliary excretion of 131I-cholylglycyltyrosine in the rat.* Br J Anaesth, 1989. **62**(3): p. 311-5.
75. Sasportas, L.S. and S.S. Gambhir, *Imaging circulating tumor cells in freely moving awake small animals using a miniaturized intravital microscope.* PLoS One, 2014. **9**(1): p. e86759.
76. Helmchen, F., W. Denk, and J.N. Kerr, *Miniaturization of two-photon microscopy for imaging in freely moving animals.* Cold Spring Harb Protoc, 2013. **2013**(10): p. 904-13.

77. Ritsma, L., et al., *Intravital microscopy through an abdominal imaging window reveals a pre-micrometastasis stage during liver metastasis.* Sci Transl Med, 2012. **4**(158): p. 158ra145.
78. Thorling, C.A., et al., *Multiphoton microscopy and fluorescence lifetime imaging provide a novel method in studying drug distribution and metabolism in the rat liver in vivo.* J Biomed Opt, 2011. **16**(8): p. 086013.
79. Wakabayashi, H., et al., *Fundamental and clinical studies on fluorescence laparoscopy after intravenous injection of fluorescein-sodium.* Gastroenterol Jpn, 1989. **24**(6): p. 676-84.
80. Goetz, M., et al., *In vivo confocal laser endomicroscopy of the human liver: a novel method for assessing liver microarchitecture in real time.* Endoscopy, 2008. **40**(7): p. 554-62.

Figure captions

Figure 1 – Intravital multiphoton microscopy of the liver of a living rat - Montage of nine image volumes collected from the liver of a living rat 20 minutes after injection of 6 mg/kg 2 M MW rhodamine dextran (red), and 2 mg/kg sodium fluorescein (green). Each of the nine panels of this mosaic is a maximum projection of 15 images collected over a depth of 15 microns. Scale bar depicts 100 micron length. Inset shows a 3X magnification of a maximum projection of a 6 micron thick volume, showing the clear resolution of the sinusoids (red, labeled with rhodamine dextran), the hepatocyte cytosol (dim fluorescein fluorescence) and bile canaliculi (bright fluorescein fluorescence). Inset image also shows nuclei, labeled with 2 mg/kg Hoechst 33342 (blue). Figure adapted from cover figure published in Intravital, 2013, Volume 5, number 3. Used with permission.

Figure 2 – Fluorescein transport in the liver of a living rat - Sequence of multiphoton excitation fluorescence images collected from the liver of a living rat before (A), and at various times after IV injection of 2 mg/kg sodium fluorescein (green) (B - E). Nuclei were labeled by intravenous injection of 2 mg/kg Hoechst 33342 (Blue) 30 minute prior to fluorescein injection. F – Similar study conducted in a rat treated with 15 mg/kg taurolithocholate (TLC), showing impaired fluorescein transport. Each image is a maximum projection of 6 images collected through a 6 micron volume. Scale bar depicts 100 micron length. Contrast in the green channel of all panels was enhanced nonlinearly by adjusting gamma to 0.8.

Figure 3 – Additional probes suitable for labeling the liver following intravenous injection – Maximum projections of image volumes collected from the livers of living rats following intravenous injection of 2 mg/kg Hoechst (Invitrogen, Carlsbad, CA, blue) and A - 0.2 mg/kg 6-CFDA (Sigma-Aldrich, St. Louis, MO, 0.2 mg/kg, green), B - 0.5 mg/kg CLF (Syncom, Groningen, Netherlands, green), C – 0.4 mg/kg CGamF (WuXi AppTec, Tianjin, China, green), D – 2 mg/kg sodium fluorescein (Sigma-Aldrich, St. Louis, MO, green) and 4mg/kg propidium iodide (Invitrogen, Carlsbad, CA). Image shown in panel D was collected from the liver of a rat 3 hours after intraperitoneal injection with 1 g/kg acetaminophen. Necrotic cells are apparent from the purple-

white labeling of nuclei resulting from the combination of Hoechst (blue) and propidium iodide (yellow to red). Scale bar depicts 100 micron length.

Figure 4 – Schematic diagram of the arrangement of a rat for intravital microscopy using an inverted microscope - Following surgery, the liver is exteriorized and attached to a coverslip-bottomed dish, which is inserted into the stage insert on the stage of inverted microscope. Imaging is conducted from below using a water immersion objective. Body temperature is maintained using warming pads placed under and over the animal, and by an objective heater wrapped around the microscope objective. Figure adapted from figure previously published in Intravital (Babbey et al., 2012). Used with permission.

Figure 5 – Stabilization of the rat liver for high-resolution intravital microscopy – A – Maximum projection of 139 sequential images of Hoechst-labeled nuclei collected over a period of approximately 2.5 minutes from the liver of a living rat. B - "XT" maximum projection of the region enclosed in the red box in panel A, in which the horizontal dimension shows the distribution of projected fluorescence across the region and the vertical dimension shows the distribution over time. Scale bar depicts 100 micron length. Contrast in both panels was enhanced non-linearly by adjustment of gamma to 0.87.

Figure 6 – The effects of vertical motion can be mitigated by maximum projection of image volumes – A – Single image collected from the liver of a living rat following IV injection of 2 mg/kg sodium fluorescein. B – Maximum projection of the 6 plane, 6 micron thick volume collected from the same field. C – Quantifications of integrated fluorescence in 4 regions-of-interest placed over segments of bile canaliculi, obtained from a series of individual images. D – Quantifications of integrated fluorescence in 4 regions-of-interest placed over segments of bile canaliculi, obtained from a series of projected image volumes. Scale bar depicts 50 micron length. The time series of individual images and projected volumes is shown in **Video 2**. Figure previously published in Intravital (Babbey et al., 2012). Used with permission.

Figure 7 – Measurements of fluorescein transport in individual hepatocytes in vivo – The mean fluorescence was measured over time in regions of interest in the cytosol (crosses), bile canaliculi (open

circles) and adjacent sinusoids (closed circles) for hepatocytes in a control rat (A) or in a rat 30 min after intravenous injection of 15 mg/kg TLC (B). Values are presented as means ± SEM. Data were obtained from the images shown in Video 1. Note that the plateau in canaliculi measurements obtained from the control animal result from detector saturation. Figure modified from version previously published in American Journal of Physiology (Regulatory, Integrative and Comparative Physiology) (Ryan et al., 2014). Used with permission.

Figure 8 – Automated generation of regions-of-interest for quantitative analyses of hepatic transport - Automated methods of digital image analysis were applied to original projected image volumes (panel A, CGamF displayed in green, Hoechst-labeled nuclei displayed in blue) to automatically segment regions of canaliculi (panel B) or hepatocyte cytosols (panel C) for automated quantification of the kinetics of secretion and uptake, respectively. Panel D shows canalicular regions of interest (red) and cytosolic regions of interest (white) overlaid over the original image. The nearly-complete overlap between the green canalicular fluorescence of the original image with the red signal of the segmented image (appearing as yellow) demonstrates the effective segmentation of the canalicular regions. The entire sequence of automatically-generated canalicular regions, alongside the original projected images is shown in **Video 4**. Scale bar is 50 microns in length. Visibility of nuclei in panel A was enhanced by non-linear adjustment of the intensity in the blue channel, using a gamma of 1.2.

Figure 9 - Quantitative analysis of the effect of endotoxin (LPS) on hepatic transport of fluorescein in rats - A – Maximum projection of an image volume collected from the liver of a living rat injected with rhodamine dextran (red) and fluorescein (green) 1 hour after intraperitoneal injection of 4 mg/kg endotoxin. Scale bar depicts 100 micron length. B – Quantifications of field-wise total canalicular fluorescence as a function of time after intravenous injection of sodium fluorescein for control rats (solid black symbols), rats 1 hour after endotoxin injection (solid red symbols) and rats 2 hours after endotoxin injection (open red symbols). C – Quantitative analysis of mean cytosolic fluorescence (± SEM) as a function of time after intravenous injection of sodium fluorescein for control rats (solid black symbols), rats 1 hour after endotoxin injection (solid red symbols) and rats 2 hours after endotoxin injection (open red symbols).

Figure 10 - Quantitative analysis of the effect of TLC on hepatic transport of CGamF in rats - A – Quantifications of field-wise total canalicular fluorescence as a function of time after intravenous injection of sodium fluorescein for control rats (solid black symbols) or rats 30 minutes after intravenous injection of 15 mg/kg TLC (solid red symbols). B – Quantitative analysis of mean cytosolic fluorescence (± SEM) as a function of time after intravenous injection of sodium fluorescein for control rats (solid black symbols) or rats 30 minutes after intravenous injection of 15 mg/kg TLC (solid red symbols).

Video captions

Video 1 - Fluorescein transport in the liver of a living rat - Sequence of multiphoton excitation fluorescence images collected from the liver of a living rat after intravenous injection of sodium fluorescein. Each image is a maximum projection of 6 images collected through a 6 micron volume for each time point. Video represents a 10 minute interval of time.

Video 2 - The effects of vertical motion can be mitigated by maximum projection of image volumes – Left - Series of images collected from a single focal plane of the liver of a living rat following IV injection of 2 mg/kg sodium fluorescein. Right - Series of corresponding maximum projection images of the 6 plane, 6 micron thick volume collected over time from the same field.

Video 3 – Effect of endotoxin on hepatic transport of fluorescein - Series of images collected over time from the liver of a living rat after intravenous injection of sodium fluorescein. Left – Vehicle treated rat, Right – Rat imaged two hours after intraperitoneal injection of 4 mg/kg endotoxin. Each image in these series is a maximum projection of 6 images collected through a 6 micron volume for each time point. Video represents a 10 minute interval of time.

Video 4 – Automatically generated canalicular regions of interest for quantitative analyses of hepatic transport - Left – Time series of images of the liver of a living rat following intravenous injection of CGamF. Right – Time series of the corresponding automatically-generated regions-of-interest for measurements of field-wise canalicular fluorescence.

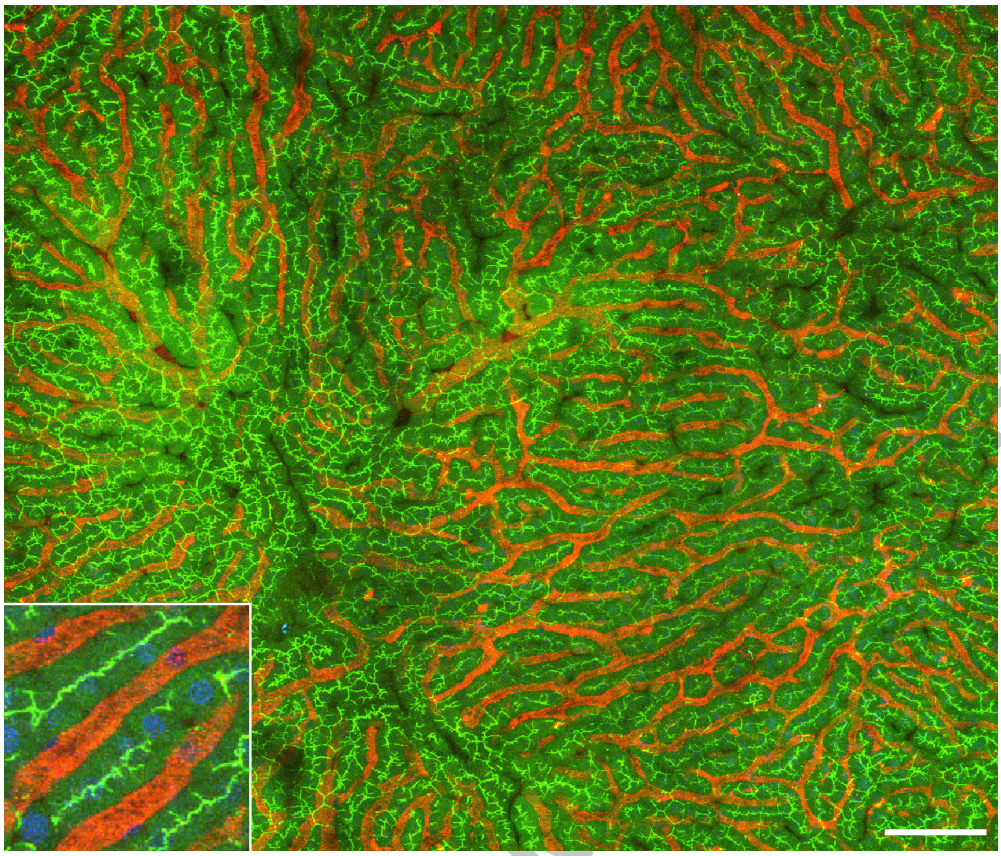

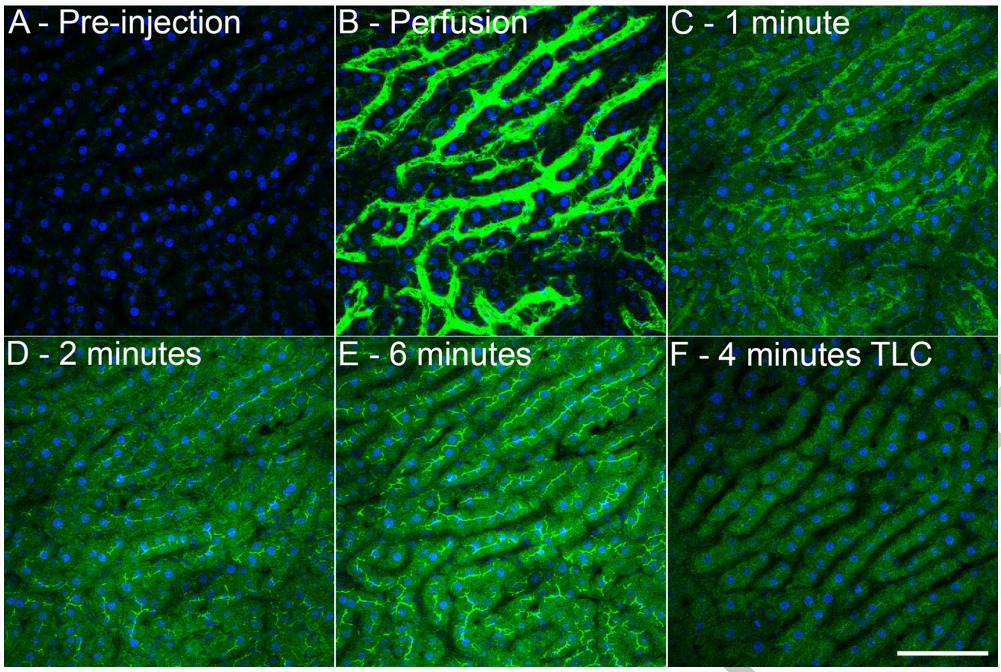

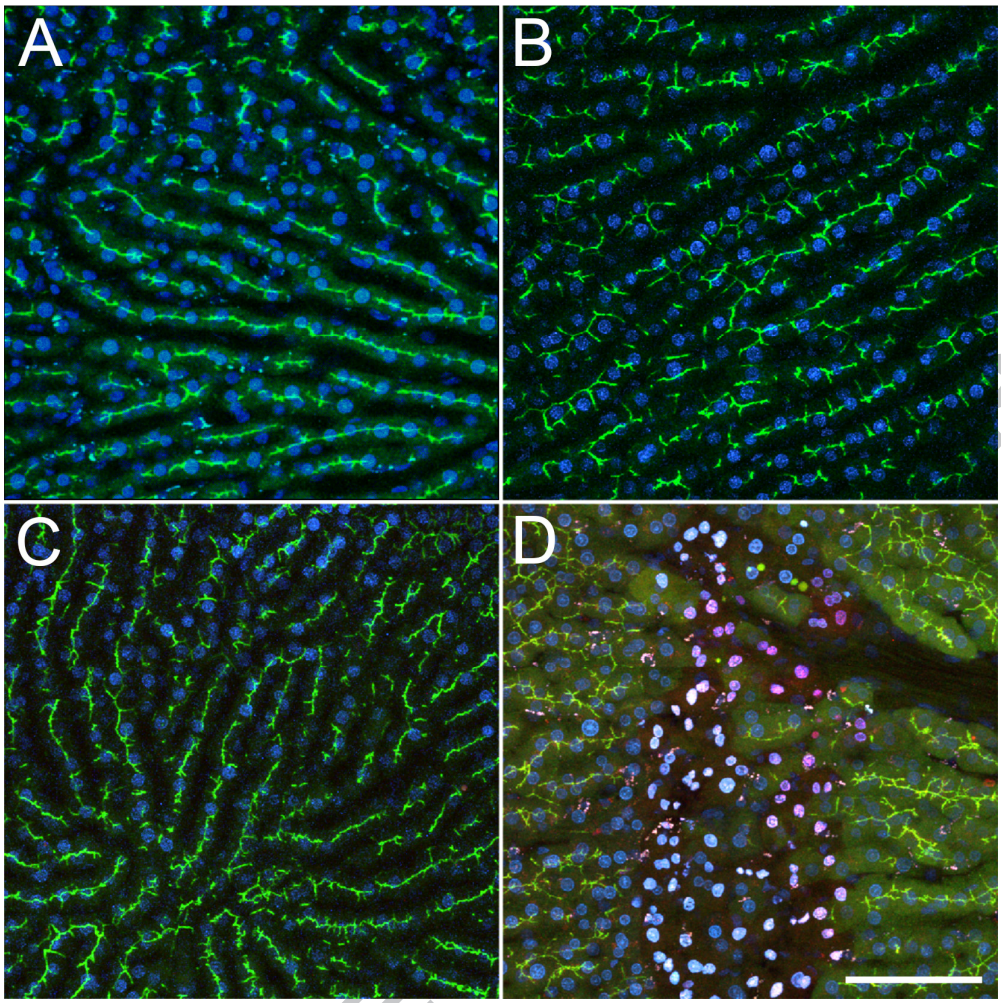

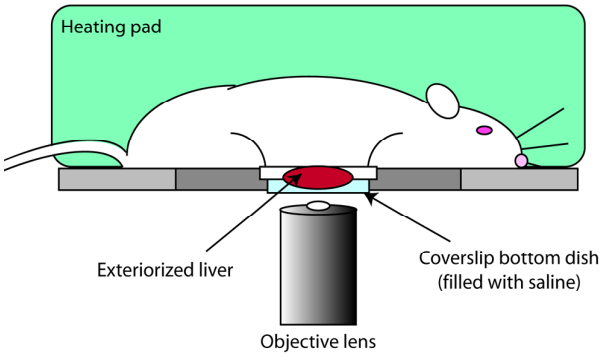

ACCEPTED MANUSCRIPT

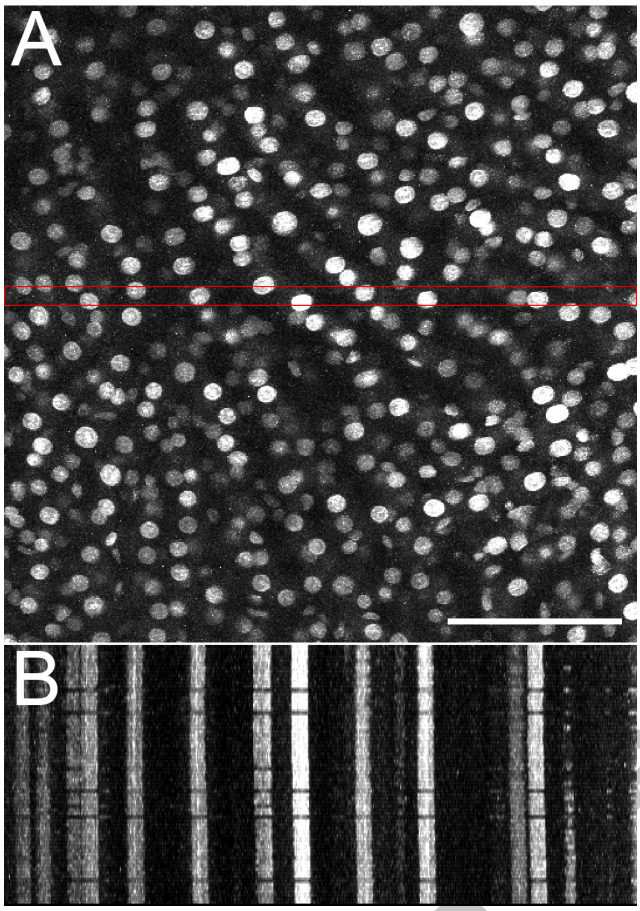

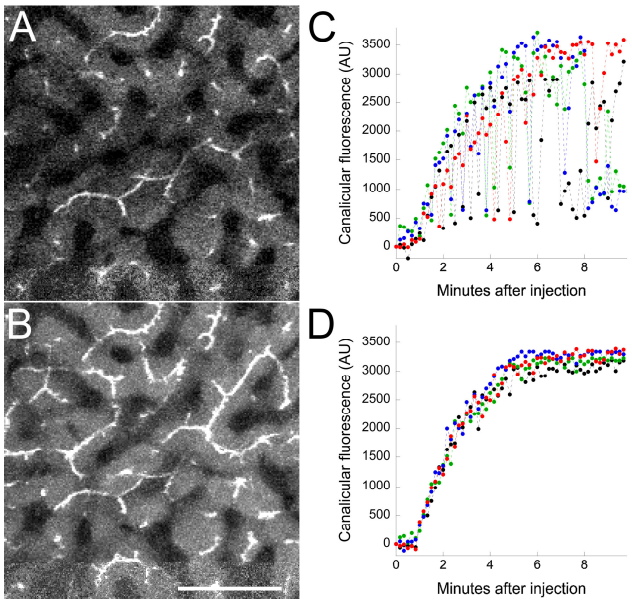

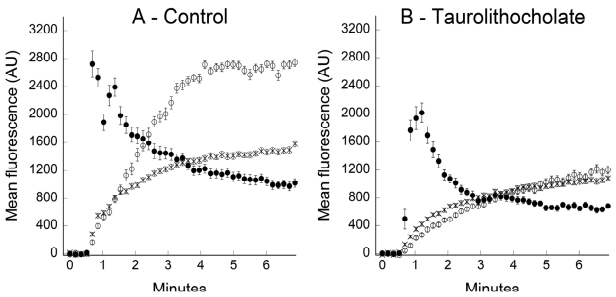

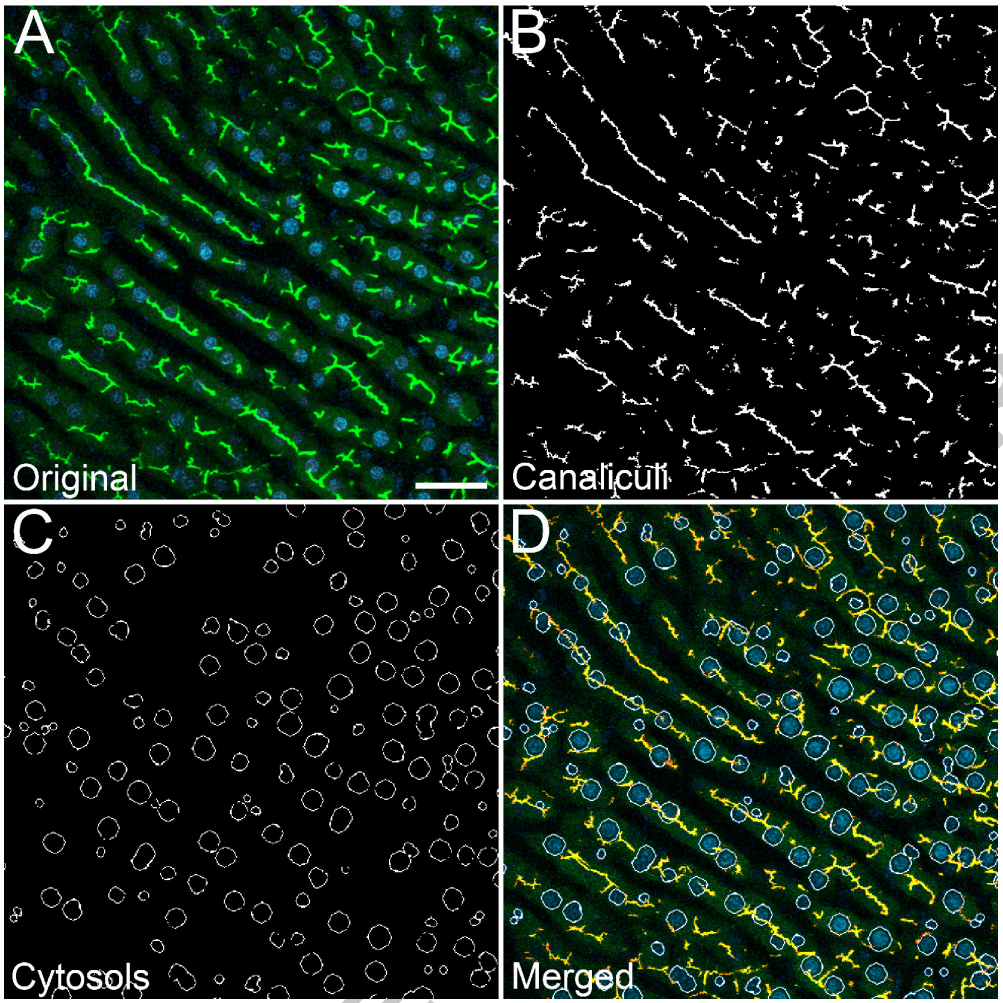

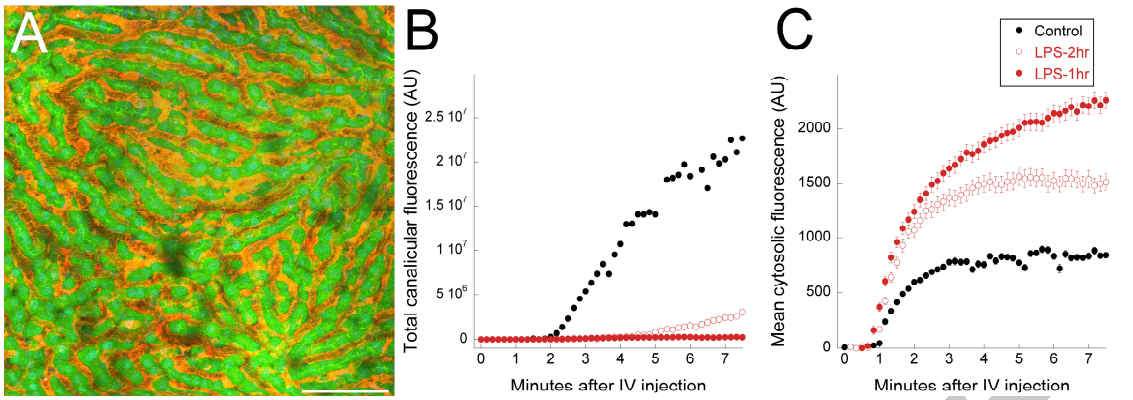

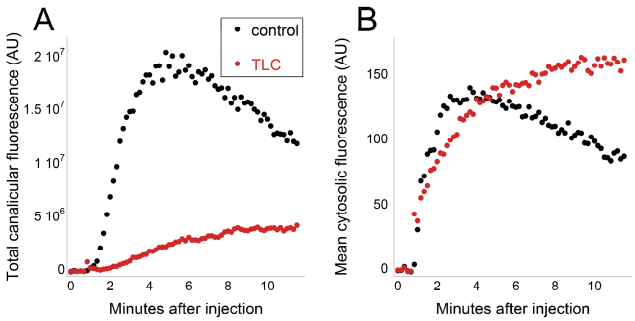

Highlights

- Hepatic transport can be characterized using microscopy of fluorescent transporter substrates.
- Multiphoton microscopy can resolve hepatic transport at subcellular resolution *in vivo*.
- Quantitative intravital microscopy can quantify disruptions in hepatic transport *in vivo*.